Materials Science & Engineering C 108 (2020) 110367

Contents lists available at ScienceDirect

Materials Science & Engineering C

journal homepage: www.elsevier.com/locate/msec

Tin disulfide nanorod-graphene-β-cyclodextrin nanocomposites for sensing dopamine in rat brains and human blood serum

Sridharan Balu[a,1], Selvakumar Palanisamy[b,c,*,1], Vijaylakshmi Velusamy[c,**], Thomas C.K. Yang[a,b,***], El-Said I. El-Shafey[d]

[a] Department of Chemical Engineering and Biotechnology, National Taipei University of Technology, No. 1, Section 3, Chung-Hsiao East Road, Taipei City, Taiwan
[b] Precision and Materials Research Centre, National Taipei University of Technology, No. 1, Section 3, Chung-Hsiao East Road, Taipei City, Taiwan
[c] Division of Electrical and Electronic Engineering, School of Engineering, Manchester Metropolitan University, Chester Street, Manchester, M1 5GD, United Kingdom
[d] Chemistry Department, College of Science, Sultan Qaboos University, P.O. Box 36, Postal Code Al-Khoudh, 123, Muscat, Oman

ARTICLE INFO

Keywords:
Graphene nanocomposite
SnS_2 nanorods
Sonochemical method
Dopamine
Guest-host chemistry
Biosensor

ABSTRACT

In the present work describes a facile synthesis of tin disulfide (SnS_2) nanorods decorated graphene-β-cyclodextrin (SnS_2/GR-β-CD) nanocomposite for robust and novel dopamine (DA) electrochemical biosensor applications. The DA biosensor was fabricated using the glassy carbon electrode (GCE) modified with SnS_2/GR-β-CD nanocomposite. The sonochemical and hydrothermal methods have been used for the synthesis of SnS_2/GR-β-CD. Different physicochemical methods were used to confirm the formation of the GR-β-CD, SnS_2, and SnS_2/GR-β-CD nanocomposite. The cyclicvoltammetric cathodic current response of DA was 5 folds higher than those observed at bare, β-CD, SnS_2-β-CD, and GR-β-CD modified GCEs. Under optimised conditions, the biosensor's DPV response current is linear to DA from the concentration of 0.01–150.76 μM. The detection limit of the biosensor was 4 nM. The SnS_2/GR-β-CD biosensor shows an excellent selectivity towards DA in the presence of common interfering species, including ascorbic acid and uric acid. Also, the as-prepared nanocomposite-modified electrode exhibited satisfactory long-term stability, sensitivity (2.49 $\mu A \mu M^{-1}$ cm^{-2}) along with reusability for detection of DA. The fabricated SnS_2/GR-β-CD biosensor was successfully used for the detection of DA in the rat brain and human blood serum samples.

1. Introduction

Over the past decades, immense attention has been paid for the fabrication of sensitive biosensors for real-time detection of dopamine (DA) neurotransmitter since it has received a substantial interest to the researchers working in analytical and biological fields [1]. Also, DA has played a vital role as a local chemical messenger and is responsible for transmitting signals to the neurons of the brain in the central nervous system (CNS) [2,3]. The range of neurological and psychiatric disorders (Parkinson's disease, attention deficit, schizophrenia, and hyperactivity disorder) are associated with the dysfunctions of DA in CNS [4,5]. The high electroactive nature of DA often can be easily detected using unmodified electrodes, such as glassy carbon and pencil graphite [6]. However, the reduced sensitivity and selectivity of unmodified glassy and graphite carbon electrodes are not suitable for the electroanalysis of DA [7]. Thus, the modified electrodes such as carbon nanotubes, graphene, polymers, and transitional metal nanoparticles/oxides have been realised for the detection of DA [8–12].

Over the past decades, 2D materials based research has become a hot topic and has been used for the wide range of applications such as detection of pathogenic bacteria, gas sensors and biomedical diagnostics [13–17]. For instance, metal oxides, graphene (GR) and metal dichalcogenides have been widely reported for various applications including construction of biosensors. Previous studies on GR based research revealed that the graphene based materials has offered more advantages in the construction of different biosensors based on DNA,

* Corresponding author. Precision and Materials Research Centre, National Taipei University of Technology, Taipei, Taiwan.
** Corresponding author.
*** Corresponding author. Department of Chemical Engineering and Biotechnology, National Taipei University of Technology, No. 1, Section 3, Chung-Hsiao East Road, Taipei City, Taiwan.
E-mail addresses: prmselva@gmail.com, S.Palanisamy@mmu.ac.uk (S. Palanisamy), V.Velusamy@mmu.ac.uk (V. Velusamy), ckyang@mail.ntut.edu.tw (T.C.K. Yang).
[1] These authors contributed equally to this work.

https://doi.org/10.1016/j.msec.2019.110367
Received 1 August 2019; Received in revised form 26 September 2019; Accepted 22 October 2019
Available online 01 November 2019
0928-4931/

peptides, proteins, enzymes and viruses [18,19]. Also, GR has been widely used as electrode modifier for detection of various chemicals owing to its enhanced physicochemical properties (surface area and conductivity) than other carbon analogues such as multiwalled nanotubes and C_{60} [20,21]. However, the direct application of pristine GR in electroanalysis is limited due to its poor selectivity in the presence of ascorbic acid (AA) and uric acid (UA). Hence, the synthesis of GR based nanocomposites has received widespread attention in electrocatalytic applications owing to their improved physiochemical properties [22]. To date, the range of functional or auxiliary materials has been used to prepare the GR hybrid nanocomposites for electroanalytical applications [21–26]. Also, various organic and inorganic compounds, including DA, can be easily electrochemically detected using the transition metal-based nanomaterials [27–31]. More recently, metal dichalcogenides have shown their promising interest in a wide range of fields due to their low cost, high surface to volume ratio and excellent stability [32,33]. Our literature survey revealed that GR-metal dichalcogenide composites have high electrocatalytic activity against the oxidation of DA at lower overpotentials than pristine GR [34–36]. Among different metal dichalcogenide, tin disulfide (SnS_2) is a layered material with CdI_2-type crystallographic structure, and arranged as S–Sn–S type structure [37]. Earlier reports suggest that the electrochemical conductivity and structural stability of SnS_2 were enhanced when integrating with active carbon material like GR [38–42]. To date, different nanostructures of SnS_2 with GR nanocomposite have been synthesized using hydrothermal and solvothermal methods [38–44]. However, in the present work, we have synthesized SnS_2 nanorods, and SnS_2 nanorods decorated GR nanocomposite using β-cyclodextrin (β-CD) as a dispersing and stabilisation agent. The unique structural characteristics of β-CD are more favourable for the formation of inclusion complexes with 2D inorganic crystals and carbon nanomaterials [45] and lead to the pathway for the establishment of SnS_2 nanorods on GR surface. For the first time, the SnS_2 nanorods decorated GR-β-CD (SnS_2/GR-β-CD) nanocomposite was used for the electroanalytical applications, and DA is used as a modal analyte to study the catalytic activity of the as-synthesized SnS_2 nanorods and the SnS_2/GR-β-CD nanocomposite.

Herein, sonochemical and hydrothermal methods were used for the synthesis of SnS_2/GR-β-CD nanocomposite. The β-CD or GR-β-CD solution are formed the inclusion complex with Sn^{4+} using the ultrasonic irradiation method. The resulting inclusion complexes with thioacetamide resulted in the formation of SnS_2 nanorods rather than SnS_2 nanoflakes. The selectivity and practicality of the SnS_2/GR-β-CD biosensor were accessed for the detection of DA.

2. Experimental

2.1. Synthesis of SnS_2/GR-β-CD nanocomposite and DA biosensor fabrication

The GR-β-CD composite was prepared by the following procedure. Briefly, about 5 mg of pristine GR (8 nm nanoflakes from Sigma) was added to the 10 mL of β-CD (10 mg mL^{-1}) aqueous solution. Double distilled (DD) water was used for the preparation of all aqueous solution. The resulting mixture was bath sonicated for 45 min using S-4000 microtip ultrasonicator probe from Misonix, Inc. (amplitude of 50% its total energy with 3-sec pulse ON and OFF). The obtained material denoted as GR-β-CD composite. Then, about 80 mg of $SnCl_4{\cdot}5H_2O$ was added into the GR-β-CD composite mixture and ultrasonicated for 10 min at room temperature. Then, the mixture moved to the magnetic stirrer, and 60 mg of thioacetamide was added and was stirred for an hour. The resulting mixture solution was transferred into a Teflon-lined stainless steel autoclave and set the temperature of 180 °C for 24 h. Once the reaction over, the obtained SnS_2/GR-β-CD nanocomposite washed with ethanol and water and dried in an air oven. The schematic design for the synthesis of SnS_2/GR-β-CD nanocomposite is shown in Fig. 1.

The SnS_2 and SnS_2-β-CD composite were also prepared by a similar (hydrothermal) method without GR-β-CD and GR. For the electrode modification, the as-prepared SnS_2/GR-β-CD and SnS_2-β-CD composite materials (5 mg mL^{-1}) were re-dispersed in DD water using sonication about 15 min. SnS_2 dispersion was also prepared by dispersing 5 mg of SnS_2 in 1 mL ethanol with the aid of sonication about 15 min. The SnS_2/GR-β-CD nanocomposite-modified electrode was prepared by dropping 8 μL of the as-prepared nanocomposite on pre-cleaned GCE and dried in air oven (Fig. 1). The SnS_2, SnS_2-β-CD, and GR-β-CD composite modified electrodes were prepared by drop coating (8 μL) of the corresponding compound on the GCE.

The 0.01 M DA stock solution was prepared using DA (Sigma Aldrich) with DD water. All electrochemical measurements (except pH studies) were carried out in pH 7.0 (0.1 M phosphate buffer) at room temperature (25 ± 2 °C) unless otherwise stated. The real samples stock solution was prepared using pH 7.0 as received. The electrochemical active surface area of the unmodified and SnS_2/GR-β-CD nanocomposite-modified GCEs were 0.71 and 0.102 cm^{-2} and was calculated using Randles–Sevcik equation from the cyclic voltammetric response of 1 mM K_3 $[Fe(CN)_6]^{3-/4-}$ in 0.1 M KCl.

2.2. Characterisation methods

The CHI 1205 electrochemical workstation (CH instruments, the Netherlands) with a standard 3 electrode configuration were used for the cyclic voltammetry and differential pulse voltammetry (DPV) methods. The JEOL JSM-7610F field-emission scanning electron microscope (FESEM) was used for the surface morphological characterizations of the synthesized materials. PANanalytical X'Pert PRO instrument (from Almelo, the Netherlands) was used to acquire the X-Ray diffraction (XRD) spectrum of the as-prepared composite materials. Fourier transform infrared (FTIR) spectroscopy and was done by PerkinElmer Frontier FTIR Spectrometer, UK. Raman spectra for the synthesized materials were taken using Dong Woo 500i Raman spectrometer.

3. Results and discussion

3.1. Characterisations of as-synthesized materials

The crystalline nature and the formation of SnS_2 on β-CD and GR-β-CD composite is confirmed by XRD. Fig. 2A shows the typical XRD spectra of GR (inset), SnS_2/β-CD, SnS_2/GR-β-CD nanocomposite. It can be seen from the inset of Fig. 2A that the raw GR shows the main diffraction peak (2θ) at 26.2° and is corresponding to the {002} plane of GR [46]. On the other hand, SnS_2/β-CD shows seven characteristic diffraction peaks at 15.02°, 28.3°, 32.6°, 42.1°, 50.3°, 52.3°, and 55.6°, which are arising from the pure hexagonal phase of SnS_2 (JCPDS 75–0367) [47]. The other diffraction peaks appeared in SnS_2/β-CD are related to the β-CD, including a salient peak at 12.2°. The SnS_2/GR-β-CD nanocomposite shows the similar diffraction peaks which obtained for SnS_2/β-CD and GR. However, it is interesting to note that the characteristic diffraction peak (12.2°) of β-CD in SnS_2/GR-β-CD nanocomposite appeared less intense when compared to the SnS_2/β-CD. The result indicates that the β-CD in the nanocomposite has a cage type assembly with SnS_2 and GR. The above XRD results confirmed the formation of SnS_2/β-CD and SnS_2/GR-β-CD nanocomposite.

The chemical composition of the nanocomposite was further established using the results obtained from FTIR and Raman spectroscopy. Raman spectrum of the synthesized SnS_2/GR-β-CD nanocomposite is shown in Fig. 2B. A typical characteristic peak for the presence of D and G bands at 1580 and 1592 cm^{-1} and a distinct 2D band was observed at 2682 cm^{-1} [35]. The number of defects is higher (D band) in SnS_2/GR-β-CD nanocomposite than pristine GR [46], and is due to the presence of the oxygen functional group of β-CD on GR

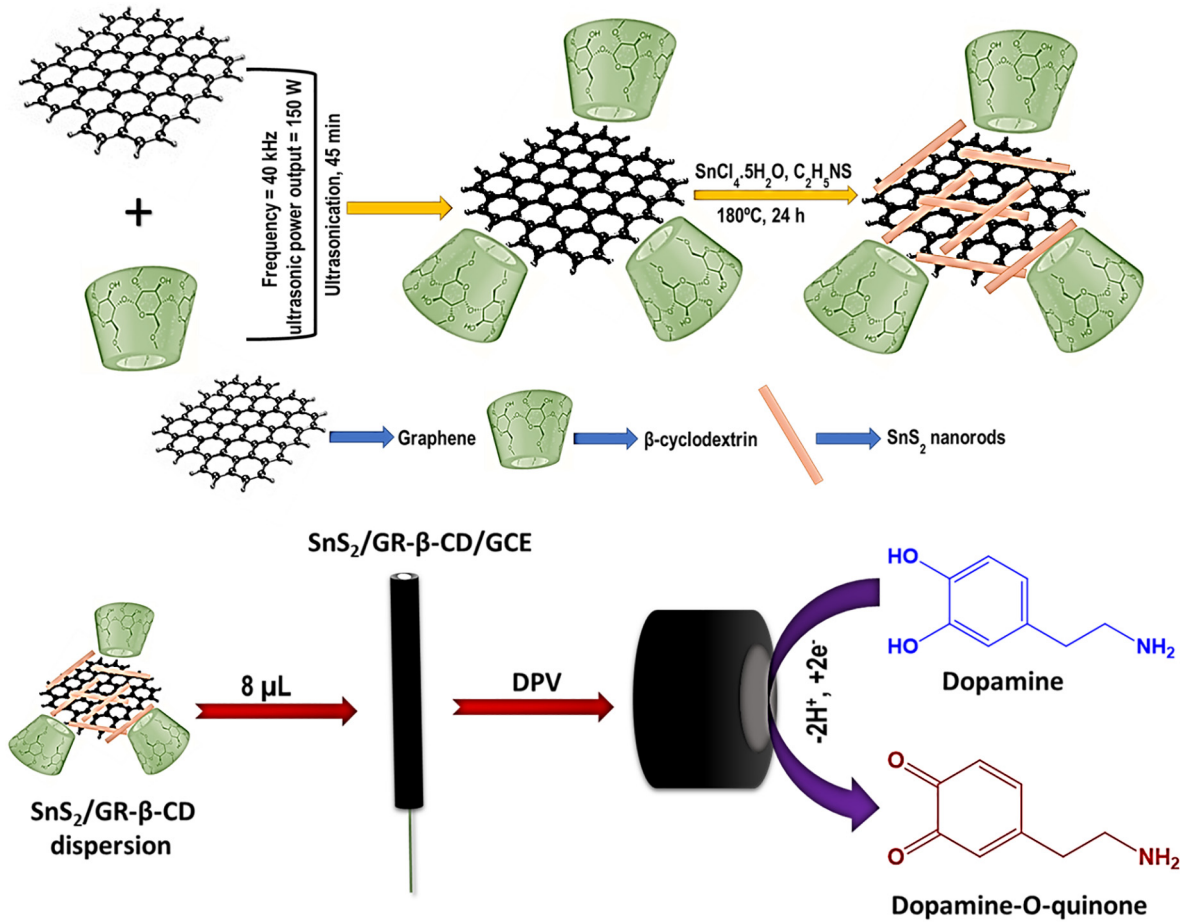

Fig. 1. The scheme of the detailed procedure for the synthesis of SnS_2/GR-β-CD nanocomposite and electrode modification and sensing of DA.

surface. The intensity ratio between 2D and G (I_{2D}/I_G) bands is 0.9, which indicates that the utilised GR in the nanocomposite is a multi-layer GR. Similarly, the GR-β-CD nanocomposite has more intense D band than the GR, which confirm the presence of more surface defects than pristine GR.

As shown in Fig. 2C, the FTIR spectra of GR is found undistinguished in the fingerprint region. On the other hand, 5 distinct vibration bands were observed at 3290 (–OH stretching), 2935 (–CH stretching), 1644 (–C═C stretching), 1362 (C–OH stretching) and 1023 cm^{-1} (C–O–C stretching) [48]. It is worthy to note that the vibration band related to –C═C stretching of GR red shifted to 1644 cm^{-1} in GR-β-CD composite, which is resulting from the durable inclusion nature of GR with β-CD. On the other hand, SnS_2/GR-β-CD nanocomposite shows a similar characteristic vibration band of GR-β-CD composite, which confirmed that there are no structural changes to GR-β-CD composite by the presence of SnS_2.

The high-resolution FESEM images of the as-prepared SnS_2/β-CD (A), SnS_2 (B), GR-β-CD (C), GR (inset of C) and SnS_2/GR-β-CD nanocomposite (D) are shown in Fig. 3. A transparent rod-like morphology of SnS_2 appeared with an average width of 40 nm on the SEM image of SnS_2/β-CD (Fig. 3A). On the other hand, a flower-like 2D flake morphology was observed for SnS_2 in the absence of β-CD (Fig. 3B), as reported early [47]. As observed from the FESEM image of SnS_2 without β-CD, the final product of SnS_2 exists in the form of 2D SnS_2 nanosheets with lateral dimensions above 100 nm. As reported earlier that the SnS_2 mostly forms 2D nanosheets rather than nanorods due to the strong covalent bonding interactions within the nanosheets. However, the van der Waals interactions between the nanosheets are much stronger after the introduction of β-CD, which is due to the durable inclusion nature of β-CD. Therefore, β-CD play a significant role in the structural transformation of SnS_2 nanorods from the flower-like 2D nanosheets. The surface morphology of GR-β-CD appears as a smooth and thin flake morphology with the association of GR nanosheets (Fig. 3C). The surface morphology of pristine GR appears as a randomly arranged 2D dense sheet like morphology (Fig. 3C inset). On the other hand, the rod-like nanostructures of SnS_2 were visible on the surface of GR-β-CD composite (Fig. 3D), and the size of the nanorods was similar to those observed for SnS_2/β-CD. The results confirm the formation of SnS_2/GR-β-CD nanocomposite.

3.2. Electrochemical detection of DA

Cyclic voltammetry was used for the detection of DA at different modified electrodes and is a preferable method to study the electrochemistry of DA. Fig. 4A shows the obtained cyclic voltammetric response of β-CD (a), GR (b), GR-β-CD (c), SnS_2 (d), SnS_2/β-CD (e) and SnS_2/GR-β-CD (f) modified GCEs in N_2 saturated pH 7.0 containing 0.15 mM DA. The detection of DA was done in the potential scanning between −0.2 to 0.7 V at a scan rate of 50 mV/s. The β-CD modified GCE shows a weak anodic peak (E_{pa}) response to DA at 0.235 V, and cathodic peak (E_{pc}) response appeared at 0.173 V. The observed anodic peak corresponds to the oxidation of DA to dopamine-o-quinone [48], and the cathodic peak is related to the reduction of oxidized dopamine-o-quinone to DA (see Fig. 6). The SnS_2 modified GCE shows 2-folds enhanced oxidation peak current (I_{pa}) response to DA than β-CD modified GCE. The E_{pa} of DA appeared at a higher potential (0.286 V) than the β-CD modified electrode. The GR modified electrode shows a broad oxidation peak to DA at 0.282 V, and was lower than those observed at β-CD and SnS_2 modified electrodes. The E_{pa} of DA dramatically reduced when the electrode modified with SnS_2/β-CD and the

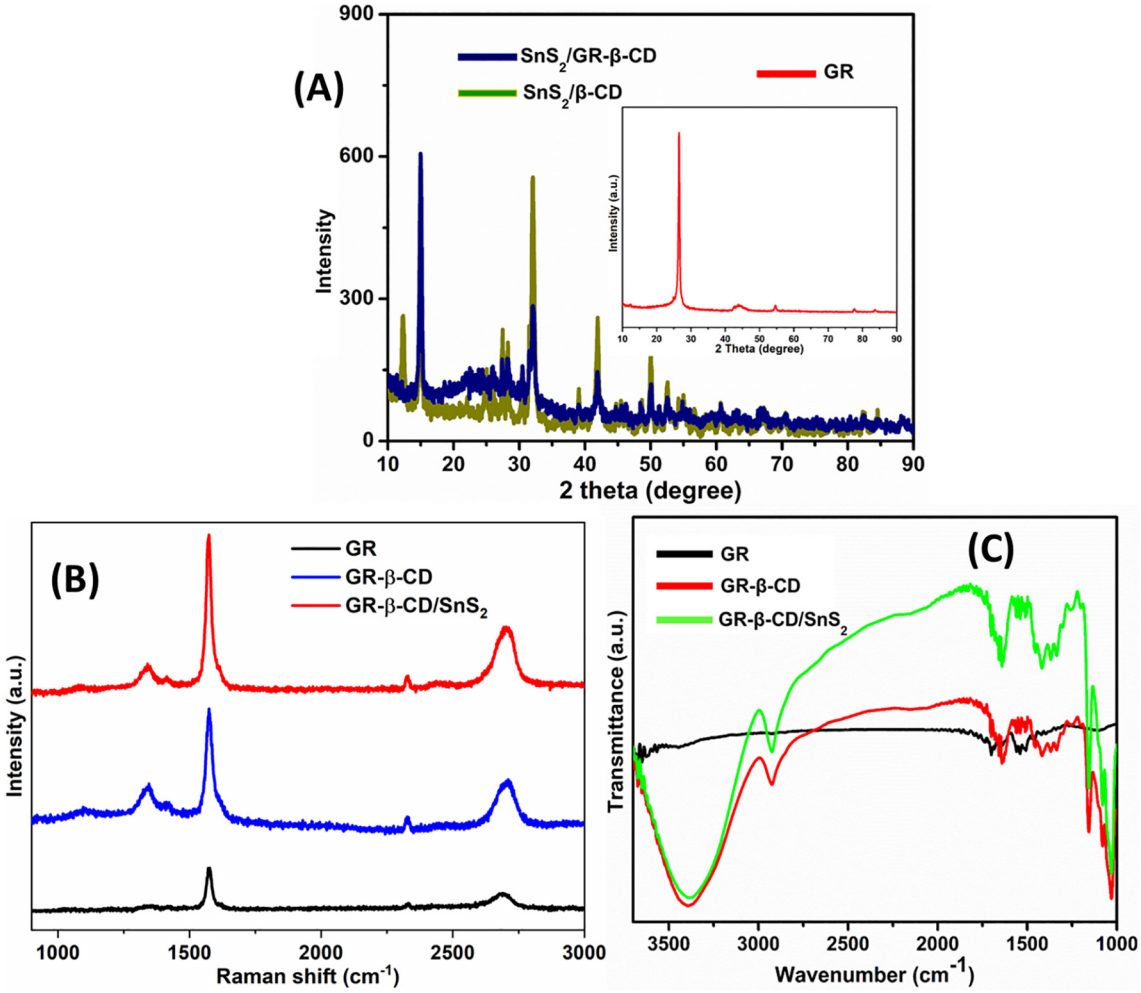

Fig. 2. A) XRD pattern of as-synthesized SnS_2/β-CD, SnS_2/GR-β-CD nanocomposite and GR (inset). B) Raman spectra of GR, GR-β-CD and SnS_2/GR-β-CD nanocomposite. C) FTIR spectra of GR, GR-β-CD and SnS_2/GR-β-CD nanocomposite.

observed E_{pa} of DA was 80 and 29 mV lower than SnS_2 and β-CD modified GCEs. At similar conditions, GR-β-CD modified GCE shows a similar catalytic activity towards DA and E_{pa} was observed at 0.204 V. However, the obtained I_{pa} of DA was lower than SnS_2/β-CD modified GCE. The peak-to-peak separation (ΔE_p, defined as (E_{pa} - E_{pc})) of SnS_2, GR, SnS_2/β-CD, and GR-β-CD modified GCEs was calculated as 106, 90, 62 and 58 mV, respectively. The result revealed that the electrochemical activity of DA was highly enhanced upon introduction of β-CD with SnS_2 and GR.

On the other hand, SnS_2/GR-β-CD nanocomposite modified GCE shows a well-defined quasi-reversible behaviour to DA, and E_{pa} and E_{pc} of DA appeared at 0.206 and 0.168 V, respectively. The ΔE_p of DA was calculated as 38 mV, which is lower than that of SnS_2, SnS_2/β-CD, and GR-β-CD modified GCEs. Also, SnS_2/GR-β-CD modified GCE shows 5 folds enhanced I_{pa} to DA than other modified GCEs. It is worthy to note that SnS_2/GR-β-CD modified GCE had higher catalytic activity and enhanced redox electrochemical behaviour to DA than other investigated electrodes. It is reported that the electrocatalytic activity of nanomaterials enhanced when they integrated with β-CD. The high catalytic activity and enhanced redox electrochemical reaction of the nanocomposite is due to the combined unique properties of SnS_2/β-CD with GR. For instance, the β-CD could quickly form an inclusion complex with DA via hydrogen bonding, and thus provides a favourable environment for the adsorption of more DA molecules on the electrode surface. Also, the high conductivity and high surface area to volume ratio of utilised SnS_2 and GR on the composite and the strong inclusion nature of β-CD with the composite and DA are resulted in the enhanced and lower potential detection of DA. The effect of drop coated amount of SnS_2/GR-β-CD nanocomposite was optimised for analytical applications since it will significantly affect the response of the DA. Fig. 4B shows the effect of different drop coated nanocomposite towards the detection of 0.15 mM DA in pH 7.0. The experimental conditions are similar to Fig. 4A. It can be seen that the nanocomposite shows a maximum response to DA at 10 μL drop coated GCE and the I_{pa} of DA was identical between 10 to 14 μL drop coated composite. Hence, 10 μL of SnS_2/GR-β-CD nanocomposite drop covered GCE was used for the analytical applications.

To further study the electrochemical behaviour of DA, the SnS_2/GR-β-CD nanocomposite-modified electrode was used for the detection of DA at different scan rates. Fig. 5A shows the cyclic voltammetry response for the redox electrochemical behaviour of DA (0.15 mM) at SnS_2/GR-β-CD nanocomposite-modified electrode in various scan rates (20–180 mV/s). A well-defined quasi-reversible redox couple of DA appeared for each scan rate from 20 to 180 mV/s (a-e). It is evident from Fig. 5A that I_{pa} and I_{pc} of DA increase with increasing the scan rates and E_{pa} and E_{pc} shifted towards a positive and negative direction. The result confirmed that the electrochemical redox behaviour of DA is mixed-kinetic process at the nanocomposite-modified electrode.[39]

To further verify the exact phenomenon, the calibration plot was plotted for the scan rate vs. I_{pa} and I_{pc} of DA (Fig. 5B). The obtained linear plot confirmed that the I_{pa} and I_{pc} of DA had a linear dependence with the scan rate from 20 to 180 mV/s. The linear regression equation

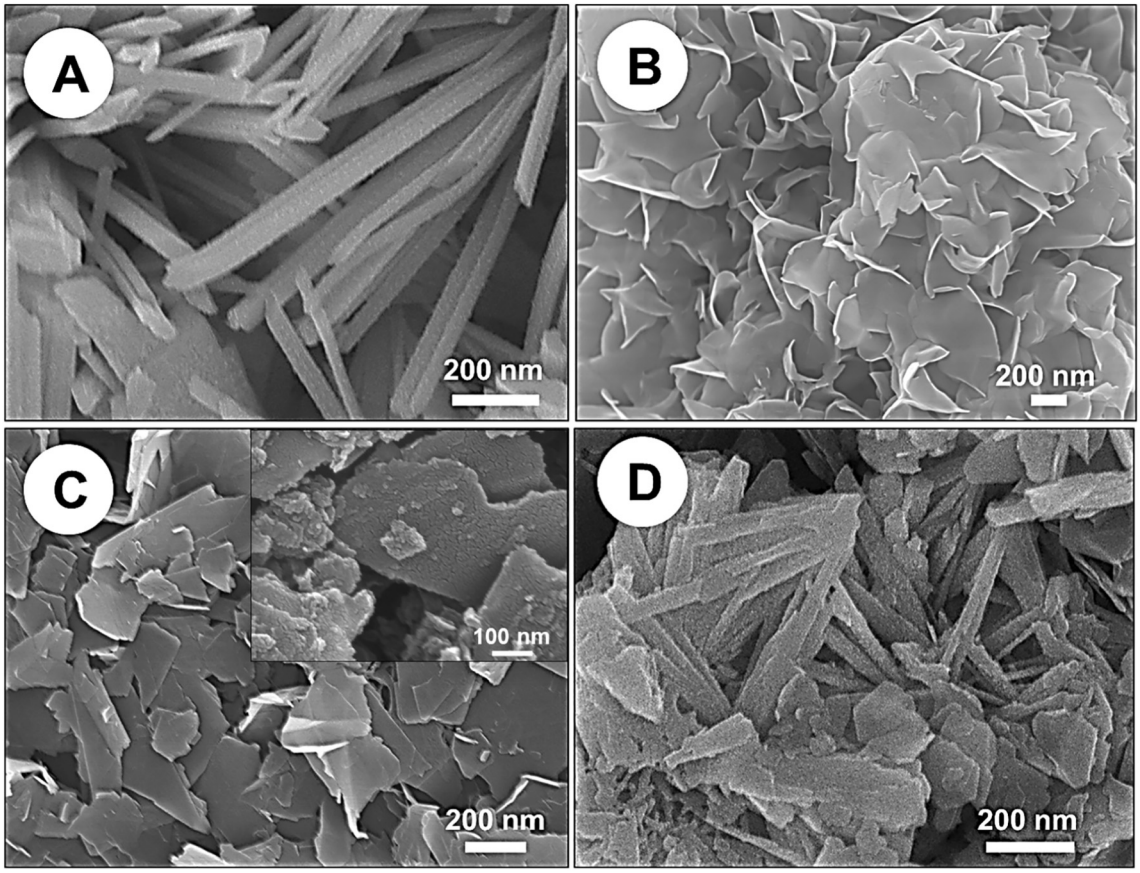

Fig. 3. High-resolution FESEM images of SnS_2/β-CD (A), SnS_2 (B), GR-β-CD (C), GR (inset of C), and SnS_2/GR-β-CD nanocomposite (D).

can written as E_{pa} (V) = 34.56ν (mV/s) + 0.2177 (R^2 = 0.9939) and E_{pc} (V) = 37.37ν (mV/s) + 2.239 (R^2 = 0.9995). The linear proportional of I_{pa} and I_{pc} with the scan rates confirmed that the redox electrochemical behaviour of DA is an adsorption-controlled electrochemical process on the nanocomposite-modified electrode surface. The effect of pH was studied using cyclic voltammetry, and the obtained voltammetric profiles are shown in Fig. 5C. The SnS_2/GR-β-CD nanocomposite-modified electrode shows a well-defined redox couple for DA (0.15 mM) in each pH. The positive and negative shift of DA potential was observed when the electrode was changed to a higher to lower pH. The result is implying that the electrons and protons are actively transferred in the electrochemical redox reaction of DA at the modified electrode. Also, a maximum profile of I_{pa} of DA was observed in pH 7.0, and the I_{pa} of DA was lowered when the electrode moves to the pH below or above 7.0. The formal potential (defined as $E^{0'} = E_{pa} + E_{pc}/2$) of DA had a linear dependence with the pH from 4.0 to 8.0, as shown in

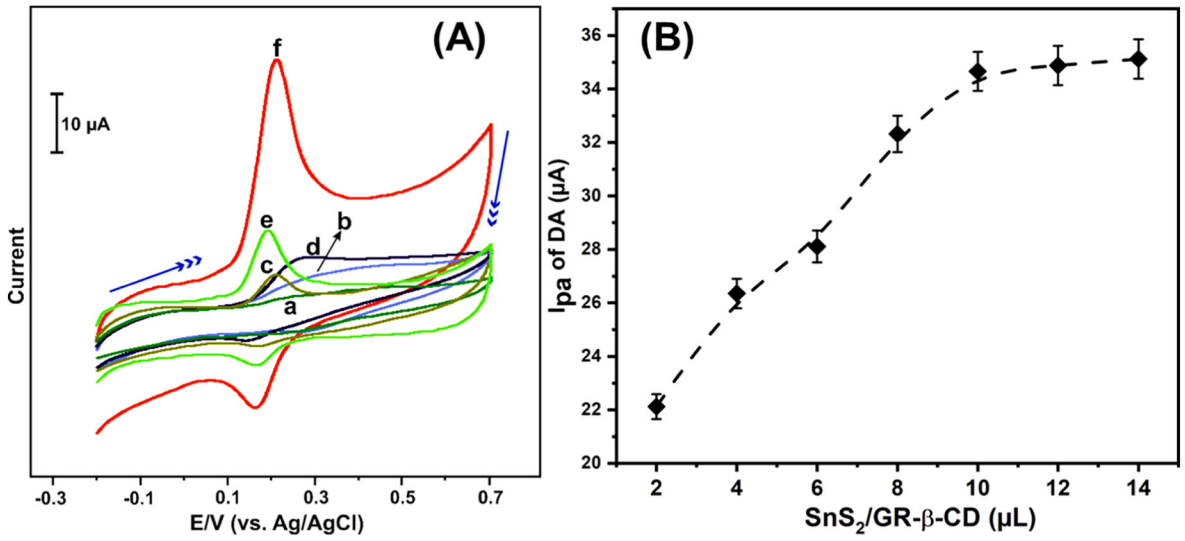

Fig. 4. A) Cyclic voltammetry response of different modified electrodes (β-CD (a), GR (b), GR-β-CD (c), SnS_2 (d), SnS_2/β-CD (e) and SnS_2/GR-β-CD (f)) in pH 7.0 solution containing 0.15 mM DA (N_2 saturated) at a scan rate of 50 mV/s. B) The effect of the oxidation peak current response for 0.15 mM DA vs SnS_2/GR-β-CD nanocomposite loading (μL) on the electrode surface. Error bar related to the 3 experiments.

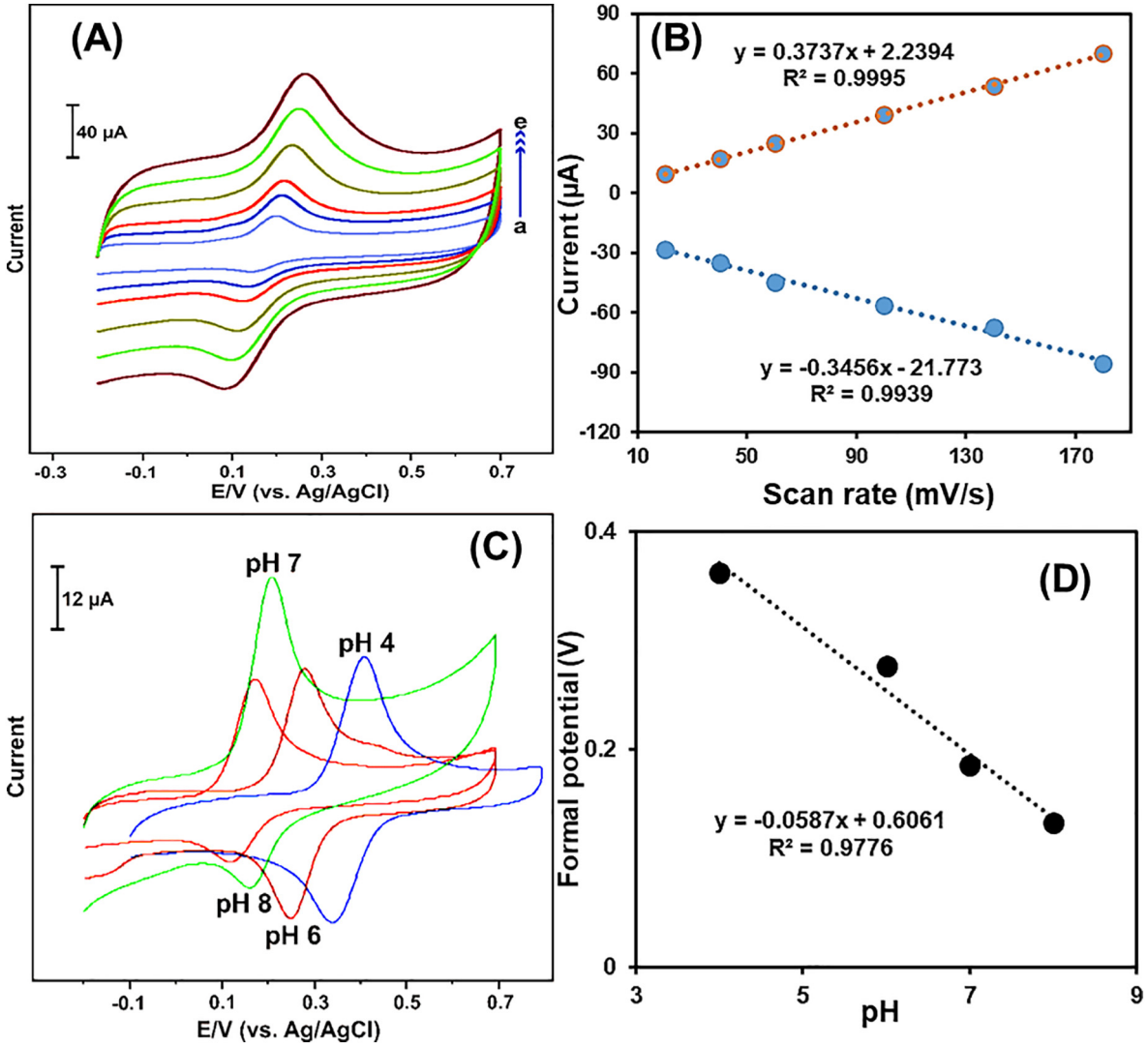

Fig. 5. A) The cyclic voltammogram obtained for SnS_2/GR-β-CD nanocomposite-modified electrode at 0.15 mM DA containing pH 7.0 solution with changing the scan rates. B) The corresponding linear plot for the scan rate vs anodic (I_{pa}) and cathodic (I_{pc}) current response of DA. C) The effect of pH on the cyclic voltammetry response of 0.15 mM DA at SnS_2/GR-β-CD nanocomposite-modified electrode at a scan rate of 50 mV/s. D) The fitted linear plot of pH vs formal potential of DA.

Fig. 5D. The corresponding linear equation for pH vs. $E^{0'}$ is $E^{0'}$ (V) = −0.0587 V/pH + 0.6061, (R^2 = 0.9776). The slope value of −58.7 mV/pH is identical to the reported theoretical value (−59.0 mV/pH) for the electrochemical redox reaction. Hence, the redox electrochemistry of DA is an equal number of electrons, and protons transferred reaction [49]. The electrochemistry of DA has already been well discussed, and a simplified possible electrochemical mechanism of DA at the SnS_2/GR-β-CD nanocomposite-modified electrode is shown in Fig. 6.

3.3. Determination of DA

The electrochemical determination of DA was done by using DPV with 30 s as an optimum incubation time for the modified electrode. The experiments were carried out by using an initial E = −0.2 V, final E = 0.7 V, amplitude = 0.05 V, pulse width = 0.05 s, sampling width = 0.2 s and pulse period = 0.2 s. Fig. 7A shows a typical DPV response of SnS_2/GR-β-CD nanocomposite-modified electrode (10 µL coated) for the absence and presence of different concentrations of DA (0.01–180.76 µM) in pH 7.0. It can be seen that the SnS_2/GR-β-CD nanocomposite-modified electrode shows a clear DPV response at 0.182 V for the addition of 10 nM of DA (curve b) and the current response increase with the further nM additions of DA (c-h) into the pH 7.0 (Fig. 7A **inset**). The result is indicating the high catalytic activity of the nanocomposite-modified electrode towards DA even in lower concentrations. It is also worthy to note that the SnS_2/GR-β-CD nanocomposite-modified electrode did not show (curve a of Fig. 7A **inset**) any apparent response in the absence of DA. The result confirmed that the electrochemical non-active nature of the nanocomposite electrode in the scanned potential at pH 7.0.

As shown in Fig. 7A, the DPV current response increases with increasing the concentration of DA. The calibration plot of [DA] vs DPV current response (Fig. 7B) reveals that the response current of DA is linearly proportional to the [DA]. The sensor had a linear dependence with the DA from the concentrations of 0.01–150.76 µM and corresponding linear equation is $I_{pa} = 1.1376\,C + 0.2536$ (R^2 = 0.9905). The sensitivity of the sensor was calculated (slope of the calibration plot/active surface area of the nanocomposite-modified electrode) as 2.49 $\mu A \mu M^{-1}\ cm^{-2}$. The limit of detection (LOD) of the sensor was calculated to be 4 nM using S/N = 3. The obtained LOD is well below the concentration of extracellular DA levels in the CNS (10–30 nM). Hence, the fabricated sensor can be used for the possible detection of DA in biological fluids. Also, the analytical results of the sensor (LOD and linear response range) is superior when compared with previously

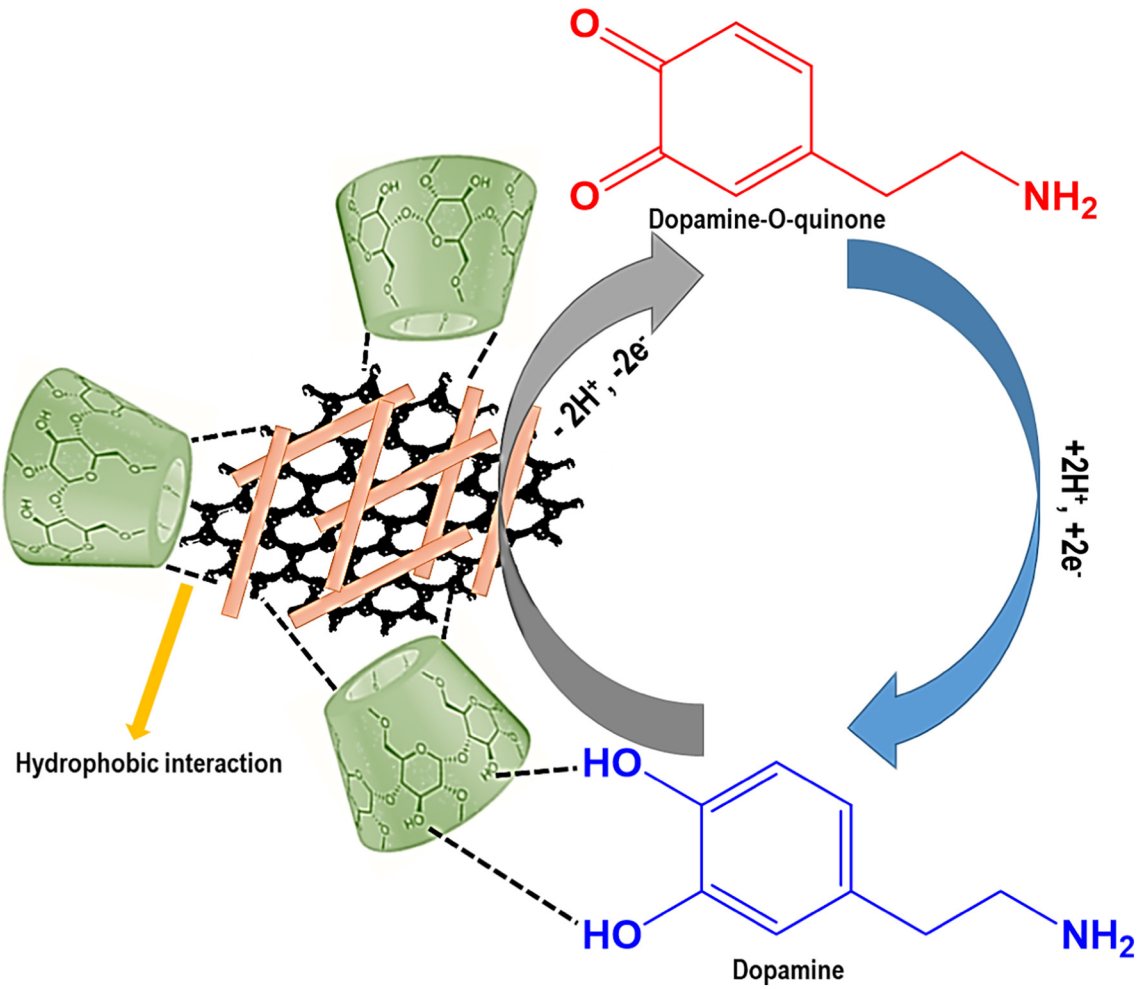

Fig. 6. The possible interaction and the mechanism for electrochemical redox reaction of DA at SnS_2/GR-β-CD nanocomposite modified electrode (the picture is not to scale).

reported GR and metal dichalcogenide based composite electrodes [34,35,50–59] for the detection of DA, as shown in Table 1. The above discussions confirmed that the SnS_2/GR-β-CD nanocomposite-modified electrode could be used as a sensitive electrode material for the low-level detection of DA.

The practical feasibility of the sensor mainly relies on the selectivity of the fabricated electrode since DA can easily co-reacts with other potentially interfering compounds. For instance, the concentration of AA in Plasma is 4–8.8 μg/mL when compared to the DA concentration (0–30 pg/mL). Hence, the selectivity of the SnS_2/GR-β-CD nanocomposite-modified electrode towards the detection of 500 nM DA was examined in the presence of 50 folds (25 μM) addition of AA, UA, epinephrine (EP), norepinephrine (NEP), hydroquinone (HQ) and catechol (CC). As can be seen from the DPV profiles, the investigated interfering compounds did not show much effect on the response current of DA (Fig. 7C). The DA can be easily interacting with β-CD and SnS_2 through hydrogen bonding, and electrostatic interactions, which results in the high selectivity of DA on GR-β-CD/SnS_2 modified electrode. Also, high surface to volume ratio of SnS_2 on GR-β-CD surface facilitate the enhanced electron-transfer towards electrode surface. It is interesting to note that the oxidation potential of DA appeared at quite lower potential (0.182 V) than the investigated interfering compounds such as UA, EP, NEP, HQ and CC (Fig. 7D). However, the high concentration of AA showed a moderate impact on the response current of DA, which is due to closer oxidation potential of AA where the DA oxidized [**60**]. The above-discussed interfering compounds did not have any impact on the detection potential and sensitivity of DA, which reveals that the DA had no cross-reactivity with interfering compounds. The above discussions confirmed that the SnS_2/GR-β-CD nanocomposite-modified electrode could be used for selective detection of DA in the blood serum samples as well as in pharmaceutical and biological samples.

The practical feasibility of the SnS_2/GR-β-CD nanocomposite was further examined for detection of DA content in rat brain and blood serum samples. The modified electrode was directly used to determining the DA concentration in rat brain and human blood serum samples, and were used without any further dilution. Also, the rat brain and blood serum samples with a known concentration of DA-containing pH 7.0 were tested using the nanocomposite-modified electrode.

The DPV was used for the real sample analysis and was performed by the scanning from −0.2 V to 0.7 V with pulse width and a pulse time of 50 and 200 mS. The standard addition method was used for the calculation of recovery of DA in the rat brain and blood serum with DA (100 nM) samples. The DA concentration in rat brain sample was predetermined as 40 nM (by DPV), and was well matched with a previously reported method [**54**]. A known concentration of DA (100 nM) was added into the real samples and was tested using the prepared nanocomposite sensor. The obtained recovery of DA in rat brain and human serum samples were listed in Table 2. The as-prepared sensors showed a recovery of 99.2% with a relative standard deviation (RSD) of 3.2%. The results confirmed that the SnS_2/GR-β-CD nanocomposite electrode could be used for practical applications.

The stability of the SnS_2/GR-β-CD nanocomposite-modified electrode towards the detection of DA was investigated using DPV. The DPV

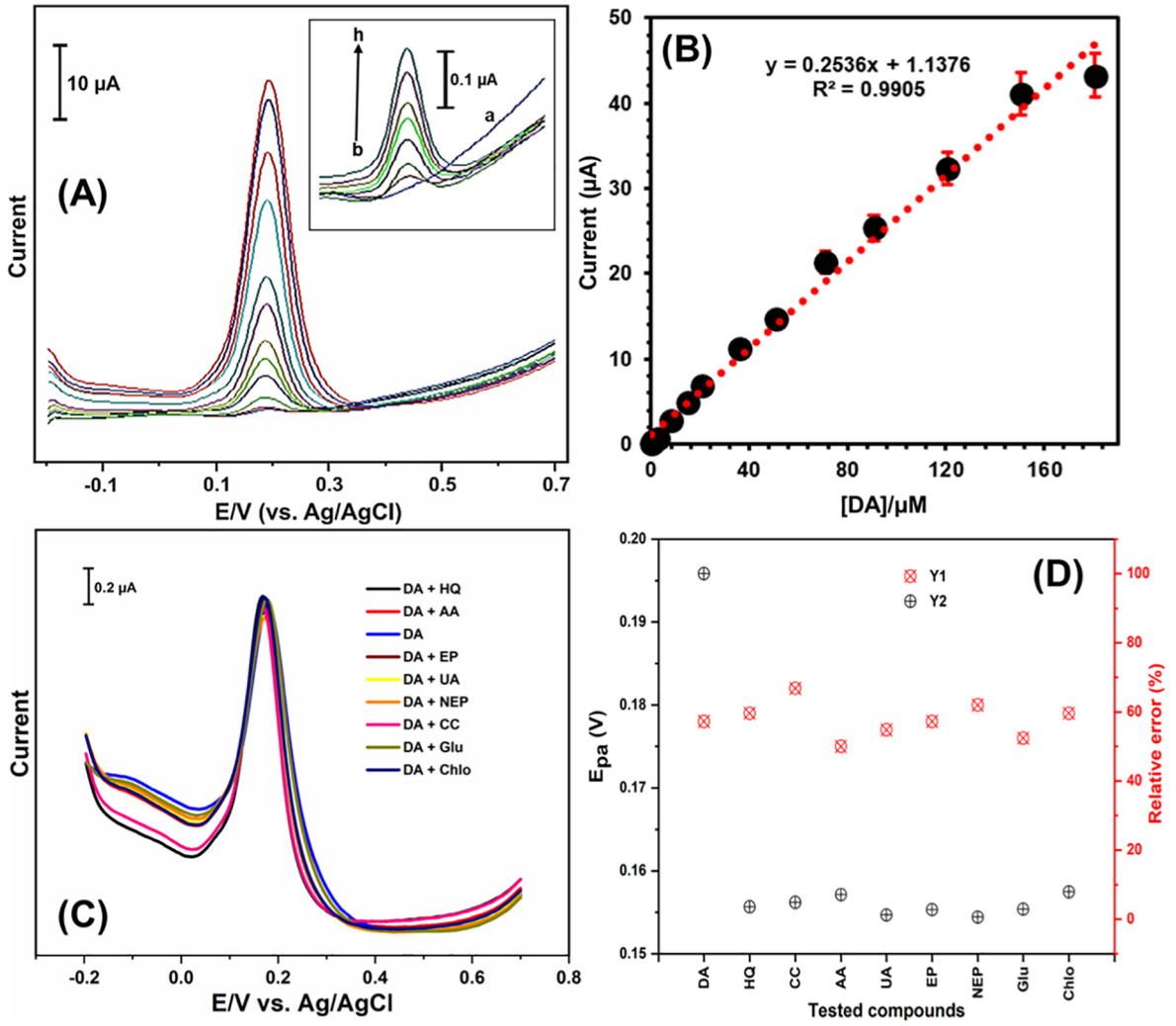

Fig. 7. A) Typical DPV responses of SnS_2/GR-β-CD nanocomposite modified electrode for the presence of different concentrations of DA in pH 7.0. The inset shows the DPV response of SnS_2/GR-β-CD nanocomposite modified electrode for the absence (a) and presence of diffrent concentrations of DA (b–h) in pH 7.0. B) The calibration plot for [DA] vs current response of DA. C) The DPV response of SnS_2/GR-β-CD nanocomposite-modified electrode for the detection of 0.5 µM DA and 25 µM addition of interfering compounds such as hydroquinone (HQ), catechol (CC), ascorbic acid (AA), uric acid (UA), epinephrine (EP) and norepinephrine (NEP) into the pH 7.0. D) The related oxidation potential of DA (YI) and relative error (Y2).

Table 1
Comparison of analytical performances (linear response range and LOD) of the SnS_2/GR-β-CD nanocomposite-modified electrode with the previously reported modified electrodes towards the determination of DA.

Modified electrode	Detection method	Linear range (µM)	LOD (nM)	Ref.
MoS_2-RGO/GCE	DPV	1.0–110.0	940.0	[34]
GR-CNT/MoS_2/GCE	DPV	0.1–100.0	50.0	[35]
CS-GR/GCE	DPV	1.0–24.0	1000.0	[50]
GR/GCE	Amperometry	4.0–100.0	2640.0	[51]
AuNPs/MoS_2/GCE	DPV	0.05–30.0	50.0	[52]
MWCNT/GONR/GCE	Amperometry	0.15–12.15	80.0	[53]
C60-GO/GCE	DPV	0.02–73.5	8.0	[54]
S-GR/GCE	DPV	0.2–20.0	20.0	[55]
ERGO/GCE	DPV	0.5–60.0	500.0	[56]
PPy-Ag-PVP/GCE	Amperometry	0.01–0.09	12.6	[57]
β-CD/Au-GR/GCE	DPV	0.5–120.0	24.0	[58]
SnS_2/CNT-CS/GCE	DPV	1.0–50.0	70.0	[59]
CuHCC/GCE	DPV	0.1–350.0	19.0	[60]
SnS_2/GR-β-CD/GCE	DPV	0.01–150.76	4.0	Present work

response of 0.5 µM DA on SnS_2/GR-β-CD nanocomposite-modified electrode (experimental conditions are similar to Fig. 7A) was monitored periodically over 2 weeks (figure not shown), and electrode was stored in dry condition when not in use. The SnS_2/GR-β-CD nanocomposite-modified electrode retains 96.2 and 89.1% of the initial sensitivity of DA. The result confirmed that the fabricated SnS_2/GR-β-CD nanocomposite-modified electrode has good storage stability towards the detection of DA.

Table 2
Determination of DA in the rat brain and human blood serum samples using as-synthesized SnS_2/GR-β-CD nanocomposite-modified electrode. RSD = 3 measurements. *Rat brain sample; **Human blood serum sample.

Sample	Added (nM)	Found (nM)	Recovery (%)	RSD (%)
RBS* (A)	0.0	40.0	–	2.6
	100.0	138.9	99.2	3.2
HBSS**	40.0	39.6	99.0	2.9
	100.0	139.1	99.3	2.7

4. Conclusions

In conclusion, a simple and straightforward strategy has been used for the synthesis of novel SnS_2/GR-β-CD nanocomposite. The surface morphological characterizations confirmed the formation of SnS_2 nanorods on GR-β-CD composite. The applicability of either SnS_2 nanorods or SnS_2/GR-β-CD nanocomposite towards the application of the electrochemical sensor has been studied for the first time. Electrochemical studies revealed that the SnS_2/GR-β-CD nanocomposite-modified electrode has better electrocatalytic activity towards DA than other investigated electrodes, including SnS_2 and GR-β-CD. The combined synergistic effects of β-CD with SnS_2/GR leads to the enhanced sensitivity and lower potential detection of DA. The SnS_2/GR-β-CD nanocomposite-modified electrode shows a lower LOD of 4 nM with wider linear response ranges up to 150.76 μM. The sensor showed excellent selectivity for DA in the presence of 50 fold additions of potentially active interfering compounds. This study confirmed that the SnS_2/GR-β-CD nanocomposite could be used as a promising electrode material for sensitive and low-level detection of DA in real samples. The sensor showed excellent recovery (99.2%) of DA in the rat brain real samples. Also, the as-synthesized nanocomposite can be used for the fabrication of other electrochemical sensors and energy devices shortly.

Declaration of competing interest

We confirm that there are no conflicts to declare.

Acknowledgements

This project was supported by the Ministry of Science and Technology (project No: 106-2119-*M*-027-001) of Taiwan. This work was jointly sponsored by the Engineering and Materials Research Centre (EMRC), School of Engineering, Manchester Metropolitan University, Manchester, UK. Authors also would like to acknowledge the Precision analysis and Materials Research Center, National Taipei University of Technology for providing the all-necessary Instrument facilities.

References

[1] B. Si, E. Song, Recent advances in the detection of neurotransmitters, Chemosensors 6 (2018) 1.
[2] A. Gröger, R. Kolb, R. Schäfer, U. Klose, Dopamine reduction in the substantia nigra of Parkinson's disease patients confirmed by in vivo magnetic resonance spectroscopic imaging, PLoS One 9 (2014) e84081.
[3] H. Braak, K.D. Tredic, U. Rüb, R.A. de Vos, S.E.N. Jansen, E. Braak, Staging of brain pathology related to sporadic Parkinson's disease, Neurobiol. Aging 24 (2003) 197–211.
[4] C.B. Jacobs, M.J. Peairs, B.J. Venton, Review: carbon nanotube based electrochemical sensors for biomolecules, Anal. Chim. Acta 662 (2010) 105–127.
[5] A. Azadbakht, M. Roushani, A.R. Abbasi, S. Menati, Z. Derikvand, A label-free aptasensor based on polyethyleneimine wrapped carbon nanotubes in situ formed gold nanoparticles as signal probe for highly sensitive detection of dopamine, Mater. Sci. Eng. C 68 (2016) 585–593.
[6] B. Thirumalraj, S. Palanisamy, S.M. Chen, R.S. Kannan, Alumina polished glassy carbon electrode as a simple electrode for lower potential electrochemical detection of dopamine in its sub-micromolar level, Electroanalysis 28 (2016) 425–430.
[7] Y.L. Su, C.Y. Tai, J.M. Zen, A simple method to tune up screen-printed carbon electrodes applicable to the design of disposable electrochemical sensors, Electroanalysis 25 (2013) 2539–2546.
[8] Y. Wang, Y. Li, L. Tang, J. Lu, J. Li, Application of graphene-modified electrode for selective detection of dopamine, Electrochem. Commun. 11 (2009) 889–892.
[9] A. Liu, I. Honma, H. Zhou, Simultaneous voltammetric detection of dopamine and uric acid at their physiological level in the presence of ascorbic acid using poly (acrylic acid)-multiwalled carbon-nanotube composite-covered glassy-carbon electrode, Biosens. Bioelectron. 23 (2007) 74–80.
[10] S. Palanisamy, P.Y. Fan, S.M. Chen, V. Velusamy, J.M. Hall, Facile preparation of a cellulose microfibers–exfoliated graphite composite: a robust sensor for determining dopamine in biological samples, Cellulose 24 (2017) 4291–4302.
[11] E.B. Bustos, M.G.G. Jiménez, B.R.D. Sánchez, E. Juaristi, T.W. Chapman, L.A. Godínez, Glassy carbon electrodes modified with composites of starburst-PAMAM dendrimers containing metal nanoparticles for amperometric detection of dopamine in urine, Talanta 72 (2007) 1586–1592.
[12] F. Li, J. Song, H. Yang, S. Gan, Q. Zhang, D. Han, A. Ivaska, L. Niu, One-step synthesis of graphene/SnO_2 nanocomposites and its application in electrochemical supercapacitors, Nanotechnology 20 (2009) 455602.
[13] G.S. Anand, A. Sivanesan, M.R. Benzigar, G. Singh, A.I. Gopalan, A.V. Baskar, H. Ilbeygi, K. Ramadass, V. Kambala, A. Vinu, Recent progress on the sensing of pathogenic bacteria using advanced nanostructures, Bull. Chem. Soc. Jpn. 92 (2019) 216–244.
[14] Q. Ji, I. Honma, S.M. Paek, M. Akada, J.P. Hill, A. Vinu, K. Ariga, Layer-by-layer films of graphene and ionic liquids for highly selective gas sensing, Angew. Chem. Int. Ed. 49 (2010) 9737–9739.
[15] N. Joshi, T. Hayasaka, Y. Liu, H. Liu1, O.N. Oliveira Jr., L. Lin, A review on chemiresistive room temperature gas sensors based on metal oxide nanostructures, graphene and 2D transition metal dichalcogenides, Micro 185 (2018) 213.
[16] C.N.R. Rao, K. Pramoda, Borocarbonitrides, BxCyNz, 2D nanocomposites with novel properties, Bull. Chem. Soc. Jpn. 92 (2019) 441–468.
[17] L. Wang, A. Wu, G. Wei, Graphene-based aptasensors: from molecule–interface interactions to sensor design and biomedical diagnostics, Analyst 143 (2018) 1526–1543.
[18] L. Wang, Y. Zhang, A. Wu, G. Wei, Designed graphene-peptide nanocomposites for biosensor applications: a review, Anal. Chim. Acta 985 (2017) 24–40.
[19] D. Li, W. Zhang, X. Yu, Z. Wang, Z. Su, G. Wei, When biomolecules meet graphene: from molecular level interactions to material design and applications, Nanoscale 8 (2016) 19491–19509.
[20] P. Edward Randviir, A.C. Dale, Brownson, C.E. Banks, A decade of graphene research: production, applications and outlook, Mater. Today 17 (2014) 426–432.
[21] A. Nag, A. Mitra, S.C. Mukhopadhyay, Graphene and its sensor-based applications: a review, Sens. Actuators, A 270 (2018) 177–194.
[22] S.J.R. Neale, E.P. Randviir, A.S.A. Dena, C.E. Banks, An overview of recent applications of reduced graphene oxide as a basis of electroanalytical sensing platforms, Appl. Mater. Today 10 (2018) 218–226.
[23] H. Teymourian, A. Salimi, S. Khezrian, Development of a new label-free, indicator-free strategy toward ultrasensitive electrochemical DNA biosensing based on Fe_3O_4 nanoparticles/reduced graphene oxide composite, Electroanalysis 29 (2017) 409–414.
[24] S. Ponnaiah, P. Prakash, B. Vellaichamy, A new analytical device incorporating a nitrogen doped lanthanum metal oxide with reduced graphene oxide sheets for paracetamol sensing, Ultrason. Sonochem. 44 (2018) 196–203.
[25] B. Vellaichamy, S. Ponnaiah, P. Prakash, A new in-situ synthesized ternary CuNPs-PANI-GO nano composite for selective detection of carcinogenic hydrazine, Sens. Actuators, B 245 (2017) 156–165.
[26] S. Palanisamy, C. Karuppiah, S.M. Chen, C.Y. Yang, P. Periakaruppan, Simultaneous and selective electrochemical determination of dihydroxybenzene isomers at a reduced graphene oxide and copper nanoparticles composite modified glassy carbon electrode, Anal. Methods 6 (2014) 4271–4278.
[27] Y. Wang, X. Qing, Q. Zhou, Y. Zhang, Q. Liu, K. Liu, W. Wang, M. Li, Z. Lu, Y. Chen, D. Wang, The woven fiber organic electrochemical transistors based on polypyrrole nanowires/reduced graphene oxide composites for glucose sensing, Biosens. Bioelectron. 95 (2017) 138–145.
[28] Z. Li, L. Sheng, A. Meng, C. Xie, K. Zhao, A glassy carbon electrode modified with a composite consisting of reduced graphene oxide, zinc oxide and silver nanoparticles in a chitosan matrix for studying the direct electron transfer of glucose oxidase and for enzymatic sensing of glucose, Microchim. Acta 183 (2016) 1625–1632.
[29] X. Yang, Y. Ouyang, F. Wu, Y. Hu, Y. Ji, Z. Wu, Size controllable preparation of gold nanoparticles loading on graphene sheets@cerium oxide nanocomposites modified gold electrode for nonenzymatic hydrogen peroxide detection, Sens. Actuators, B 238 (2017) 40–47.
[30] Y. Xu, W. Zhang, J. Shi, X. Zou, Y. Li, E.T. Haroon, X. Huang, Z. Li, X. Zhai, X. Hu, Electrodeposition of gold nanoparticles and reduced graphene oxide on an electrode for fast and sensitive determination of methylmercury in fish, Food Chem. 237 (2017) 423–430.
[31] H. Terrones, F.L. Urías, M. Terrones, Novel hetero-layered materials with tunable direct band gaps by sandwiching different metal disulfides and diselenides, Sci. Rep. 3 (2013) 1549.
[32] L. Ruitao, A. Joshua, Robinson, E. Raymond, Schaak, S. Du, S. Yifan, E.Thomas Mallouk, T. Mauricio, Transition metal dichalcogenides and beyond: synthesis, properties, and applications of single- and few-layer nanosheets, Acc. Chem. Res. 48 (2015) 56–64.
[33] H.Y. Yue, S.S. Song, S. Huang, H. Zhang, X.P.A. Gao, X. Gao, X.Y. Lin, L.H. Yao, E.H. Guan, H.J. Zhang, Preparation of MoS_2-graphene hybrid nanosheets and simultaneously electrochemical determination of levodopa and uric acid, Electroanalysis 29 (2017) 2565–2571.
[34] K. Pramoda, K. Moses, U. Maitra, C.N.R. Rao, Superior performance of a MoS_2-RGO

composite and a borocarbonitride in the electrochemical detection of dopamine, uric acid and adenine, Electroanalysis 27 (2015) 1892–1898.
[35] V. Mani, M. Govindasamy, S.M. Chen, R. Karthik, S.T. Huang, Determination of dopamine using a glassy carbon electrode modified with a graphene and carbon nanotube hybrid decorated with molybdenum disulfide flowers, Microchim. Acta 183 (2016) 2267–2275.
[36] L. Mei, C. Xu, T. Yang, J. Ma, L. Chen, Q. Li, T. Wang, Superior electrochemical performance of ultrasmall SnS_2 nanocrystals decorated on flexible RGO in lithium-ion batteries, J. Mater. Chem. A 1 (2013) 8658–8664.
[37] A. Samad, M.N.A. Alam, Y.H. Shin, First principles study of a SnS_2/graphene heterostructure: a promising anode material for rechargeable Na ion batteries, J. Mater. Chem. A 4 (2016) 14316–14323.
[38] L. Zhuo, Y. Wu, L. Wang, Y. Yu, X. Zhang, F. Zhao, One-step hydrothermal synthesis of SnS_2/graphene composites as anode material for highly efficient rechargeable lithium ion batteries, RSC Adv. 2 (2012) 5084–5087.
[39] J. Zheng, X. Xiong, G. Wang, Z. Lin, X. Ou, C. Yang, M. Liu, SnS_2 nanoparticles anchored on three-dimensional reduced graphene oxide as a durable anode for sodium ion batteries, Chem. Eng. J. 339 (2018) 78–84.
[40] H. Sun, M. Ahmad, J. Luo, Y. Shi, W. Shen, J. Zhu, SnS_2 nanoflakes decorated multiwalled carbon nanotubes as high performance anode materials for lithium-ion batteries, Mater. Res. Bull. 49 (2014) 319–324.
[41] P. Zheng, Z. Dai, Y. Zhang, K.N. Dinh, Y. Zheng, H. Fan, J. Yang, R. Dangol, B. Li, Y. Zong, Q. Yan, X. Liu, Scalable synthesis of SnS_2/S-doped graphene composites for superior Li/Na-ion batteries, Nanoscale 9 (2017) 14820–14825.
[42] W. Deng, X. Chen, Z. Liu, A. Hu, Q. Tang, Z. Li, Y. Xiong, Three-dimensional structure-based tin disulfide/vertically aligned carbon nanotube arrays composites as high-performance anode materials for lithium ion batteries, J. Power Sources 277 (2015) 131–138.
[43] Y. Jiang, Y. Guo, W. Lu, Z. Feng, B. Xi, S. Kai, J. Zhang, J. Feng, S. Xiong, Rationally incorporated MoS_2/SnS_2 nanoparticles on graphene sheets for lithium-ion and sodium-ion batteries, ACS Appl. Mater. Interfaces 9 (2017) 27697–27706.
[44] K. Sudip, Batabyala, C. Basua, G.S. Sanyalb, A.R. Das, Synthesis of Sb_2Se_3 nanorod using β-cyclodextrin, Mater. Lett. 58 (2003) 169–171.
[45] B. Thirumalraj, S. Palanisamy, S.M. Chen, K.D. Wael, A graphene/gelatin composite material for the entrapment of hemoglobin for bioelectrochemical sensing applications, J. Electrochem. Soc. 163 (2016) B265–B271.
[46] Y. Du, Z. Yin, X. Rui, Z. Zeng, X.J. Wu, J. Liu, Y. Zhu, J. Zhu, X. Huang, Q. Yan, H. Zhang, A facile, relative green, and inexpensive synthetic approach toward large-scale production of SnS_2 nanoplates for high-performance lithium-ion batteries, Nanoscale 5 (2013) 1456–1459.
[47] S. Balu, K. Uma, G.T. Pan, T.C.K. Yang, S.K. Ramaraj, Degradation of methylene blue dye in the presence of visible light using SiO_2@α-Fe_2O_3 nanocomposites deposited on SnS_2 flowers, Materials 11 (2018) 1030.
[48] S. Palanisamy, S. Sakthinathan, S.M. Chen, B. Thirumalraj, T.H. Wu, B.S. Lou, X. Liu, Preparation of β-cyclodextrin entrapped graphite composite for sensitive detection of dopamine, Carbohydr. Polym. 135 (2016) 267–273.
[49] V.K. Ponnusamy, V. Mani, S.M. Chen, W.T. Huang, J. Jen, Rapid microwave assisted synthesis of graphene nanosheets/polyethyleneimine/gold nanoparticle composite and its application to the selective electrochemical determination of dopamine, Talanta 120 (2014) 148–157.
[50] D. Han, T. Han, C. Shan, A. Ivaska, L. Niu, Simultaneous determination of ascorbic acid, dopamine and uric acid with chitosan-graphene modified electrode, Electroanalysis 22 (2010) 2001–2008.
[51] Y.R. Kim, S. Bong, Y.J. Kang, Y. Yang, R.K. Mahajan, J.S. Kim, H. Kim, Electrochemical detection of dopamine in the presence of ascorbic acid using graphene modified electrodes, Biosens. Bioelectron. 25 (2010) 2366–2369.
[52] H. Sun, J. Chao, X. Zuo, S. Su, X. Liu, L. Yuwen, C. Fan, L. Wang, Gold nanoparticle-decorated MoS_2 nanosheets for simultaneous detection of ascorbic acid, dopamine and uric acid, RSC Adv. 4 (2014) 27625–27629.
[53] C.L. Sun, C.T. Chang, H.H. Lee, J. Zhou, J. Wang, T.K. Sham, W.F. Pong, Microwave-assisted synthesis of a Core–Shell MWCNT/GONR heterostructure for the electrochemical detection of ascorbic acid, dopamine, and uric acid, ACS Nano 5 (2011) 7788–7795.
[54] B. Thirumalraj, S. Palanisamy, S.M. Chen, B.S. Lou, Preparation of highly stable fullerene C60 decorated graphene oxide nanocomposite and its sensitive electrochemical detection of dopamine in rat brain and pharmaceutical samples, J. Colloid Interface Sci. 462 (2016) 375–381.
[55] S.J. Li, J.H. He, M.J. Zhang, R.X. Zhang, X.L. Lu, S.H. Li, H. Pang, Electrochemical detection of dopamine using water-soluble sulfonated graphene, Electrochim. Acta 102 (2013) 58–65.
[56] L. Yang, D. Liu, J. Huang, T. You, Simultaneous determination of dopamine, ascorbic acid and uric acid at electrochemically reduced graphene oxide modified electrode, Sens. Actuators, B 193 (2014) 166–172.
[57] B. Vellaichamy, P. Periakaruppan, T. Paulmony, Evaluation of a new biosensor based on in situ synthesized ppy-ag-pvp nanohybrid for selective detection of dopamine, J. Phys. Chem. B 121 (2017) 1118–1127.
[58] Z. Chang, Y. Zhou, L. Hao, Y. Hao, X. Zhu, M. Xu, Simultaneous determination of dopamine and ascorbic acid using b-cyclodextrin/Au nanoparticles/graphene-modified electrodes, Anal. Methods 9 (2017) 664–671.
[59] Y. Pan, Y. Zhang, Y. Li, Layer-by-layer self-assembled multilayer films of single-walled carbon nanotubes and tin disulfide nanoparticles with chitosan for the fabrication of biosensors, J. Appl. Polym. Sci. (2013) 647–652.
[60] N. Karikalan, M. Velmurugan, S.M. Chen, K. Chelladurai, A copper hexacyanocobaltate nanocubes based dopamine sensor in the presence of ascorbic acid, RSC Adv. 6 (2016) 48523–48529.